

From 2D to 3D: Bridging Self-Assembled Monolayers to a Substrate-Induced Polymorph in a Molecular Semiconductor

Yansong Hao, Gangamallaiiah Velpula, Martin Kaltenegger, Wolfgang Rao Bodlos, François Vibert, Kunal S. Mali, Steven De Feyter, Roland Resel, Yves Henri Geerts, Sandra Van Aert, David Beljonne, and Roberto Lazzaroni*



Cite This: *Chem. Mater.* 2022, 34, 2238–2248



Read Online

ACCESS |



Metrics & More

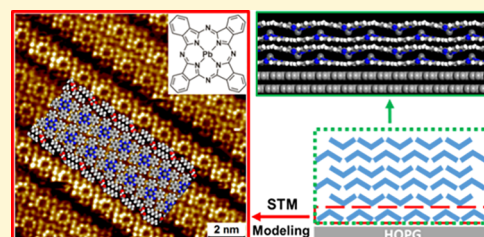


Article Recommendations



Supporting Information

ABSTRACT: In this study, a new bottom-up approach is proposed to predict the crystal structure of the substrate-induced polymorph (SIP) of an archetypal molecular semiconductor. In spite of intense efforts, the formation mechanism of SIPs is still not fully understood, and predicting their crystal structure is a very delicate task. Here, we selected lead phthalocyanine (PbPc) as a prototypical molecular material because it is a highly symmetrical yet nonplanar molecule and we demonstrate that the growth and crystal structure of the PbPc SIPs can be templated by the corresponding physisorbed self-assembled molecular networks (SAMNs). Starting from SAMNs of PbPc formed at the solution/graphite interface, the structural and energetic aspects of the assembly were studied by a combination of in situ scanning tunneling microscopy and multiscale computational chemistry approach. Then, the growth of a PbPc SIP on top of the physisorbed monolayer was modeled without prior experimental knowledge, from which the crystal structure of the SIP was predicted. The theoretical prediction of the SIP was verified by determining the crystal structure of PbPc thin films using X-ray diffraction techniques, revealing the formation of a new polymorph of PbPc on the graphite substrate. This study clearly illustrates the correlation between the SAMNs and SIPs, which are traditionally considered as two separate but conceptually connected research areas. This approach is applicable to molecular materials in general to predict the crystal structure of their SIPs.



1. INTRODUCTION

Polymorphism represents the ability of compounds to crystallize into different forms. These crystal forms are called polymorphs and usually differ in atomic arrangement or molecular packing. Studying polymorphism is of prime importance since it determines the physical properties of materials, such as solubility, mechanical properties, and electronic properties,^{1–3} with major impacts in different areas, for example, organic semiconducting materials,^{1,4} liquid crystalline materials,⁵ and pharmaceutical compounds.^{3,6–8}

Among all types of crystals, polymorphs of organic molecules are abundantly diverse.⁹ This is because within crystals, organic molecules interact often through weak van der Waals interactions. These polymorphs show different space groups or differ in the molecular conformations. However, a typical value for the energy difference between different polymorphs is <2 kJ/mol.^{10,11} Such large diversity and slight energy difference make it challenging to control the crystallization of organic molecules into the desired polymorph.

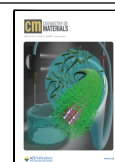
It has been well documented that the surface plays an important role in the crystallization process.^{1,12–14} The surface acts as a catalyst by lowering the activation energy barriers, which gives rise to heterogeneous crystallization.¹⁵ Beyond such catalyzing effects, some studies have reported that molecular materials can crystallize into new polymorphic forms in the

vicinity of the substrate.^{7,16–18} These new forms are called substrate-induced polymorphs (SIPs). Their structures are often distinct from those reported for the bulk phases. Earlier studies of SIPs mainly focused on organic semiconductor materials.^{19–22} The best known example is pentacene for which different SIPs are obtained as the nature of the substrate changes,^{23–25} with some of these SIPs showing improved charge transfer mobility compared to bulk forms.^{26,27} Recently, SIPs of pharmaceutical molecules also drew attention for their possible effects on bioavailability and solubility.^{7,28} Thin-film crystals are often prepared by drop casting, spin coating, or physical vapor deposition^{1,29} from which their crystal structures are determined by X-ray diffraction techniques.^{20,21,30} Despite a growing number of experimental observations,^{18,31} the formation of SIPs from the substrate is difficult to be investigated from experiments only and hence the mechanism for the formation of SIPs is still unclear.

Received: November 23, 2021

Revised: February 4, 2022

Published: February 17, 2022



SIPs typically extend vertically over at least several molecular layers; the thinnest possible SIP is the topic of another conceptually related research line: self-assembled molecular networks (SAMNs) of organic molecules, which are composed of a single layer of molecules on a solid substrate. SAMNs have been studied extensively over the past couple of decades, mostly with scanning probe microscopy, and molecular assemblies with complex architectures can be built or even manipulated.^{32–38} Such assemblies promote the development of functional surfaces with potential applications in different areas,³⁹ such as organic photovoltaics,⁴⁰ photonics,⁴¹ and host–guest chemistry.⁴² However, despite detailed experimental studies in the field of SIP and SAMN, respectively, such conceptual connection is not fully understood yet. The understanding of how the SAMN affects the crystal structure formation on top of it is still missing.

For a better comprehension of this connection, we have chosen a compound from a prototypical class of organic semiconductors, lead phthalocyanine (PbPc, Figure 1), and studied the SAMNs on highly oriented pyrolytic graphite (HOPG) as a starting point toward the possible generation of an SIP from this self-assembled network.

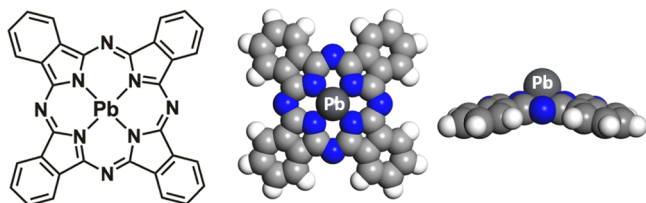


Figure 1. Molecular structure and geometry of PbPc.

PbPc shows many interesting physical and chemical properties, such as high chemical and thermal stability,⁴³ high coloring property, and photoconductivity,⁴⁴ along with promising electrical properties for use in sensors for hazardous gases.^{45–47} In addition to these electronic and optical properties, the structural features of PbPc are also interesting in the context of this study since the molecule is highly symmetric (C_{4v}) but nonplanar, in contrast to other metal phthalocyanine molecules.

Self-assembled monolayers of PbPc have first been reported on MoS_2 as deposited by molecular beam epitaxy, and the scanning tunneling microscopy (STM) data revealed three arrangements of the assembled PbPc molecules.⁴⁸ In a more recent study, PbPc monolayers were deposited onto epitaxial graphene on SiC and their internal organization was investigated by STM under ultrahigh vacuum.⁴⁹ PbPc molecules were found to be packed into a long-range ordered self-assembly with a square 2D unit cell.

It must be noted, however, that the nonplanarity of the PbPc molecule can lead to different adsorption conformations on the substrate, with the central Pb atom either pointing away (Pb-up) or toward (Pb-down) the substrate. Up to now, an unambiguous determination of the molecular adsorption conformation within the assemblies is still missing. Regarding 3D crystals, two bulk polymorphs were reported for PbPc: a monoclinic phase with the $P2_1/c$ space group⁵⁰ and a triclinic phase whose space group is $P-1$.⁵¹ To the best of our knowledge, the question of whether the SAMN of PbPc could direct its crystal structure growth into the known bulk phases or SIPs within the thin films has never been addressed.

In this study, the PbPc self-assembly was carried out at the solution/HOPG interface, instead of the common high vacuum

conditions. With this approach, self-assembled monolayers form in the presence of the solution, that is, closer to equilibrium conditions compared to vacuum deposition. After preparation, STM was employed in situ to determine the structural organization of the assembly with a resolution down to the (sub)molecular level. The adsorption conformation of the PbPc molecules was then determined unequivocally by comparing simulated and experimental STM images. In parallel to the STM measurements, force field simulations were employed in order to have a better understanding of the molecular packing within the assembly. The growth of an SIP for the PbPc molecule, as templated by the self-assembled monolayer, was then modeled by successive adsorption of up to four molecular layers. Complementarily, experimental PbPc thin films were prepared and their crystal structure was determined using X-ray diffraction techniques. In this manner, the results could be compared with the model SIP to obtain an integrated view over the 2D to 3D assembly of this molecular semiconductor.

2. METHODOLOGY

2.1. Experimental Details. **2.1.1. Self-Assembled Monolayer Preparation and STM Measurements.** A stock solution of PbPc ($C_{\text{PbPc}} = 2.9 \times 10^{-4}$ M) was prepared by dissolving appropriate amounts of the compound in 1-heptanoic acid (HA). The stock solution was diluted further with HA to prepare a concentration series. All STM experiments were performed at room temperature (21–23 °C) using a PicoSPM (Agilent) machine operating in the constant current mode with the tip immersed in the supernatant solution. STM tips were prepared by mechanically cutting a Pt/Ir wire (80%/20%, diameter 0.2 mm). Prior to imaging, a drop of the solution was placed onto a freshly cleaved surface of HOPG (grade ZYB, Advanced Ceramics Inc., Cleveland, USA). The experiments were repeated in 2–3 sessions using different tips to check for reproducibility and to avoid experimental artifacts, if any. For analysis purposes, recording of a monolayer image was followed by imaging the graphite substrate underneath under the same experimental conditions, except for increasing the current and lowering the bias. The images were corrected for drift via scanning probe image processor software (Image Metrology ApS), using the recorded graphite images for calibration purposes, allowing a more accurate unit cell determination. The unit cell parameters were determined by examining at least four images and only the average values are reported. The images were Gaussian-filtered. The imaging parameters are indicated in the figure caption: tunneling current (I_{set}) and sample bias (V_{bias}).

2.1.2. Thin-Film Preparation and X-ray Diffraction Measurements. HOPG monochromators were purchased from Momenite Performance Materials Quartz Inc. with a ZYB grade. This corresponds to an X-ray mosaic spread of 0.5–1°. The dimensions of the HOPG are 12 mm × 12 mm × 12 mm. Thin films of PbPc were prepared on HOPG via physical vapor deposition (PVD). To clean the HOPG, sticking tape was dabbed on the surface and subsequently removed. The cleaned substrates were then transferred into the high-vacuum chamber of the PVD reactor. After reaching a high vacuum in a low 10^{-6} mbar level, PbPc was sublimed from an effusion evaporator. The PbPc film growth was controlled via a microbalance.

Specular X-ray diffraction experiments on the samples were performed using an Empyrean system (Panalytical, the Netherlands) equipped with a copper sealed tube (wavelength of 0.15418 nm), a parallel mirror, beam masks, and slits, and a

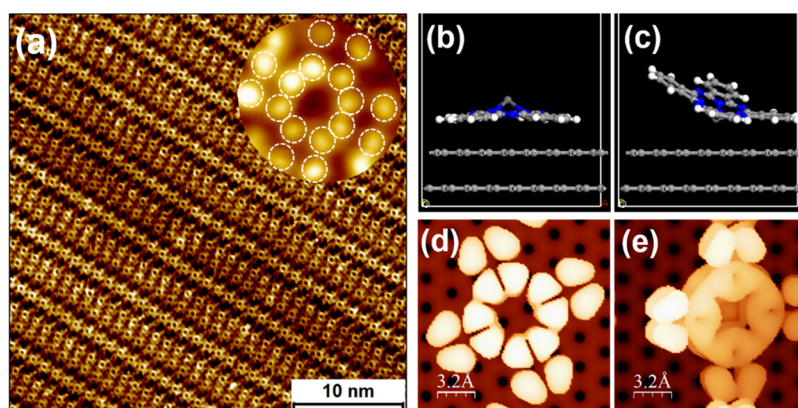


Figure 2. (a) Self-assembly of PbPc at the HA/HOPG interface with a zoomed image of a single PbPc molecule. Imaging parameters: $I_{\text{set}} = 70$ pA and $V_{\text{bias}} = -1.29$ V. Optimized atomistic models for Pb-up (b) and Pb-down (c) conformations and the corresponding simulated STM images (d and e) at the experimental bias voltage, $V = -1.29$ V.

PIXcel3D detector was used in the scanning line (1D) mode. Grazing incidence X-ray diffraction (GIXD) experiments were performed at the Elettra Synchrotron Trieste in order to study the crystal structures of the thin films. The wavelength on the beamline (XRD1) was set to 0.140 nm, and the scattering intensities were collected via a 2 M Pilatus detector. For better statistics, the sample was rotated during the measurement. Calibration was performed using LaB_6 standards. GIDVis software⁵² was used to analyze the collected data, and the corresponding GIXD pattern was indexed by GIDInd software.⁵³ During indexation, the lattice parameters were solved in a two-step procedure. In step one, two Miller indices of the contact plane between the thin-film crystal and the substrate, h and k , were determined from the observed peaks, from which the lattice parameters a , b , and γ can be calculated. Then, the third Miller index of the contact plane l and the lattice parameters c , α , and β were calculated in the second step.⁵⁴ In a subsequent step, the molecular packing was optimized in the given crystallographic unit cell by force field simulations.

2.2. Computational Details. **2.2.1. STM Simulations.** To simulate the STM images, density functional theory (DFT) calculations were carried out using the 4.1 version of the SIESTA code including periodic boundary conditions.⁵⁵ The exchange-correlation functional is described by the generalized gradient approximation in the Perdew–Burke–Ernzerhof form. A numerical double-zeta polarized atomic basis set is used for valence electrons, where the 5s, 5p, and 4d states of Pb are well described. The nuclei and core electrons are described by Troullier–Martins pseudopotentials.⁵⁶ A reasonable mesh cutoff of 250 Ry was utilized with a Monkhorst–Pack grid of $(1 \times 1 \times 1)$. Only one point is sufficient for sampling since the dimension of the unit cell of the input structure is relatively large: around 15 Å in x and y directions. For the z direction, a distance of 60 Å is used. The Grimme correction is used to account for the van der Waals (vdW) interactions.⁵⁷ All SIESTA calculations were performed on the structures obtained from the force field calculations. In SIESTA, the local density of states (LDOS) are integrated over an energy window that is determined by the experimental bias voltage used for recording the STM images. The simulated images were then generated from this LDOS based on the Tersoff–Hamann approximation by using WSxM software.⁵⁸

2.2.2. Molecular Mechanics (MM) and Dynamics (MD) Simulations. All force field calculations were performed in the Forcite module of the BIOVIA Materials Studio 2018.⁵⁹ In our

study, the classical Dreiding force field⁶⁰ was first modified in such a way that accurate descriptions for both the molecular geometry and the bulk crystal structures of PbPc are obtained. Details of the reparameterization process and the performance of the modified force field are included in the [Supporting Information](#). This modified force field was then employed in all MM/MD simulations. The atomic charges were assigned from the ESP charges calculated at the DFT level using the Gaussian 16 program package.⁶¹ For those DFT calculations, the M06-2X functional is employed, with the 6-311G(d) basis set for the C, N, and H atoms, while the LANL2DZ basis set and pseudopotential are used for the Pb atom.

The MD simulations for the PbPc assemblies were conducted in the NVT (constant number of particles, volume, and temperature) ensemble with the Nosé–Hoover–Langevin⁶² thermostat. The HOPG substrate is modeled by two graphite layers that are kept frozen during the simulations as the physisorption of molecules is not expected to affect the geometry of the substrate. The quench MD approach (see [Supporting Information](#) for more details) was used on different models for the molecular assembly. Compared to the usual MD simulations, structures are optimized periodically in time during this quench MD process. This enables a refinement of those initially optimized structures and a more efficient convergence toward the most stable structure, which is then compared with the experimental assembly.

3. RESULTS AND DISCUSSION

3.1. PbPc SAMNs: Adsorption Conformation of a Single PbPc Molecule and STM Contrast. As shown in [Figure 2a](#), PbPc forms highly ordered self-assembled monolayers upon physisorption at the HA/HOPG interface. The monolayer consists of defect-free domains that extend over several thousand square nanometers ([Figure S1](#), [Supporting Information](#)). A close inspection of the STM images reveals that each molecular row consists of PbPc molecules closely packed along the row axis and each molecule appears as a collection of 16 bright dots (see the inset in [Figure 2a](#), dots labeled by the white dashed circles).

The STM data presented in [Figure 2a](#) are somewhat unusual. The first peculiar feature of the acquired STM data is the appearance of the individual PbPc molecules. In particular, the center of the PbPc molecules, where the lead atom is located, appears as a depression. This is in contrast to the STM data

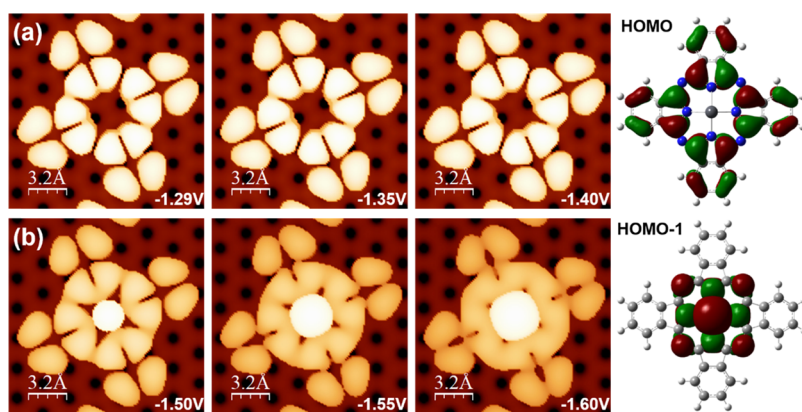


Figure 3. Simulated STM images for the Pb-up conformation at different bias voltages together with the highest occupied molecular orbital (HOMO) and HOMO-1 orbital of the PbPc molecule. The simulated STM images at the bias values used in this work and in ref ⁴⁹ are shown in panels a and b, respectively.

obtained under UHV conditions where the Pb atom appeared as a bright protrusion in the STM images.⁴⁹ Furthermore, in self-assembled networks of alkyl-substituted lead pyrenocyanine formed at the solution–solid interface, the lead atom was observed as a bright protrusion as well.⁶³ However, a few molecules in the assembly network of alkyl-substituted lead pyrenocyanine showed a depression at their molecular center and this depression was ascribed to the molecules adsorbed with a Pb-down adsorption conformation.⁶³ These observations might be related to the prevalence of either the Pb-up or the Pb-down adsorption conformation, resulting from the large size of the central metal, which does not fit inside the isoindole cavity of phthalocyanine. Tin phthalocyanine behaves similarly: depending on the orientation of the metal center, the central cavity of the molecule adsorbed on metal surfaces appeared in the STM images either as a protrusion (Sn above the molecular plane, Sn-up) or as a depression (Sn below the molecular plane, Sn-down).⁶⁴ In order to identify the factors contributing to the STM contrast of the PbPc molecules in the self-assembled network and to determine the adsorption conformation of PbPc on the graphite surface, detailed modeling studies are carried out.

The preferred adsorption conformation for a PbPc molecule on the HOPG substrate is determined from simulations. A single PbPc molecule is adsorbed in Pb-up (the lead atom points away from the substrate) or Pb-down (the lead atom points toward the substrate) conformation on the bilayer graphene, which acts as a model substrate. Both structures are then optimized by force field calculations. (Figure 2b,c, respectively). Their relative stability is then evaluated by comparing the adsorption energy, which is calculated with the following equation:

$$E_{\text{adsorption}} = E_{\text{tot}} - E_{\text{mol}} - E_{\text{substrate}}$$

where E_{tot} is the total potential energy of the optimized adsorption system, and E_{mol} and $E_{\text{substrate}}$ are the potential energies for the isolated molecule and the substrate. The adsorption energy for the Pb-up conformation is found to be -76.8 kcal/mol, while it is only -47.6 kcal/mol for the Pb-down conformation. The Pb-up conformation is clearly preferred because it maximizes the vdW interactions between the phthalocyanine ring and the HOPG substrate. In contrast, in the Pb-down conformation, only a part of the phthalocyanine ring is in close contact with the substrate leading to weaker vdW interactions.

The simulated STM images for the Pb-up and the Pb-down adsorption conformations are shown in Figure 2d,e, respectively. This enables a more direct comparison with the experimental image in order to confirm the molecular conformation within the experimental assembly. The simulated STM image for the Pb-up conformation is made up of 16 bright features, which is in line with the experimentally obtained STM image (see Figure 2a inset). Most importantly, the center of the molecule (corresponding to the position of the lead atom) appears dark compared to the periphery of the molecule. In contrast, the simulated image for the Pb-down conformation has clearly different features. An obvious brightness gradient arises over the molecule: the upper-left part of the molecule is brighter than the lower-right part, which is attributed to the inclination of the PbPc molecule, and a nonzero response is also present at the molecular center. The simulated STM image of the Pb-down adsorption conformation clearly does not match with the experimental STM data.

While the experimental and the simulated STM data obtained in this study agree closely, they differ from the experimental STM data reported recently by Nguyen et al.⁴⁹ As described above, PbPc molecules appeared with a bright central protrusion in their self-assembled network formed on graphene on SiC under UHV conditions. In order to understand this difference, and to further ascertain the adsorption conformation of PbPc in the present case, we simulated STM images at several bias voltages for the Pb-up configuration to cover the experimental conditions used in the study of Nguyen et al. and compared those data to the molecular frontier orbitals of PbPc. Note that the UHV-STM images were acquired at a bias voltage of -1.5 V,⁴⁹ whereas the STM data presented in this study are recorded at a bias voltage of -1.29 V.

Figure 3 shows a series of simulated STM images at different bias voltages together with the frontier molecular orbitals of PbPc. Clearly, the patterns of the STM images are closely related to the shape of those orbitals. It can be noticed that at a moderate bias voltage (i.e., -1.40 V or a less negative value), only the HOMO orbital of PbPc contributes to the image. Since the HOMO has a node on the central atom, brightness at the molecular center is not expected, fully consistent with the aspect of the molecules in Figure 2a. Once the bias voltage is turned to more negative values (lower than -1.5 V), additional contributions from the HOMO-1 orbital are present in the simulated image. In particular, the bright molecular center

observed in Nguyen's experiments is reproduced by our simulations. Such a bright center due to the contribution of the Pb atom is characteristic of the HOMO-1 orbital. We also find that the intensities coming from the phthalocyanine ring are increasingly smeared out as the bias voltage becomes more negative. This is associated with the contributions in the HOMO-1 orbital of the four nitrogen atoms that connect the isoindole fragments of the molecule. Combining the experimental data with all the simulated STM images, it is concluded that the PbPc molecules all have the "Pb-up" conformation in our assembly, while the aspect of the molecular center is directly related to the shape of the molecular orbitals that are probed at a given bias voltage.

3.2. Long-Range Order in PbPc SAMNs. Apart from the appearance of individual PbPc molecules in the experimental STM images, the second peculiar feature of the assembly lies in the arrangement of molecules perpendicular to the row direction. A small-scale STM image of the same domain as shown in Figure 2a is depicted in Figure 4a. It clearly shows that the assembly consists of alternating single and double rows of PbPc molecules separated by dark narrow gaps.

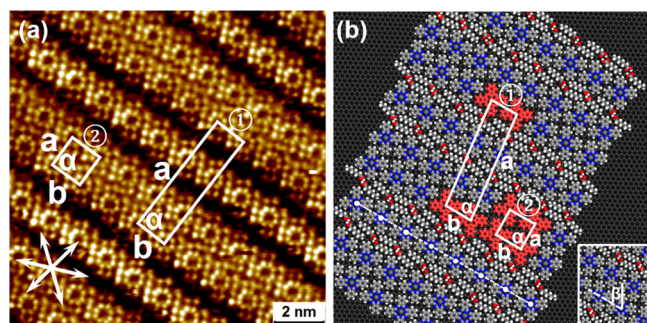


Figure 4. (a) Small-scale STM image with submolecular resolution. The graphite symmetry axes are shown in the lower left corner. The unit cells are overlaid on the STM image. Imaging parameters: $I_{\text{set}} = 70$ pA and $V_{\text{bias}} = -1.29$ V. The unit cell parameters are provided in Table 1. (b) Quench MD-refined atomistic model for the solvent coadsorbed PbPc assembly.

Within these rows, the relative orientation of molecules remains the same. Therefore, two sets of lattice parameters can be extracted from the images. The corresponding unit cells are also shown in Figure 4a: a rectangular one that encompasses the single row/double row alternation and a square one within the double rows. The lattice parameters for the rectangular unit cell are $a = 52 \pm 1$ Å, $b = 14 \pm 1$ Å, and $\alpha = 88 \pm 1^\circ$; for the square unit cell, they have dimensions of $a = b = 14 \pm 1$ Å and $\alpha = 88 \pm 1^\circ$.

Given that PbPc molecules here do not possess any peripheral functional groups, they are expected to form close-packed assemblies. In fact, when self-assembled under ultrahigh vacuum on the surface of graphene, PbPc indeed formed a close-packed self-assembled network in the absence of any gaps.⁴⁹ The formation of molecular rows separated by "dark" narrow gaps thus appears to be specific to the solution–solid interface. The reason for the formation of this particular molecular arrangement is therefore investigated by detailed force field simulations based on the hypothesis that solvent coadsorption may take place. The solvent used in our experiments is HA. Coadsorption of HA within molecular assemblies has been reported by Sirtl et al.⁶⁵ In their study, the coadsorption was inferred by comparing

assemblies prepared in high vacuum and at the solution/HOPG interface. Nevertheless, direct proof for the existence of coadsorbed solvent molecules was not reported.

The modeling study starts by building five candidate assemblies including coadsorbed solvent molecules (see Supporting Information, Figure S8) that are packed differently. Considering the structure of the HA molecule, two types of intermolecular interactions must be considered when investigating its packing: the hydrogen bond between carboxylic groups and the vdW interactions between interdigitated alkyl chains. Each of these five candidate assemblies promotes one or both of these interactions and their lattice parameters are set at the experimental values. Detailed descriptions for the building of these assemblies are provided in the Supporting Information. These candidate assemblies are first optimized by MM. After optimization, two candidate assemblies show better structural rigidity since both vdW interactions and hydrogen bonds between solvent molecules are present. These two assemblies are then expanded and refined by quench MD. A detailed comparison between these two expanded assemblies is discussed in the Supporting Information (Figure S9). The most stable and ordered assembly after refinement is shown in Figure 4b and compared to the experimental assembly.

In Figure 4b, solvent molecules between PbPc rows are paired by hydrogen bonds without disturbing the organization of the surrounding PbPc molecules. All PbPc molecules are oriented in the same way and they are perfectly aligned within the rows. Similar to the experiment, two types of unit cell are extracted and illustrated in Figure 4b. Unit cell 1 is almost rectangular with dimensions of $a = 55.3$ Å, $b = 13.8$ Å, and $\alpha = 83^\circ$, while molecules within the PbPc double rows pack into a quasi-square unit cell, namely, unit cell 2, with parameters $a = b = 13.8$ Å and $\alpha = 88.5^\circ$. Inside each molecular row, PbPc molecules are rotated with respect to the row axis by $\beta = 62 \pm 0.57^\circ$. The lattice parameters for the unit cell of the experimental assembly and the modeled assembly are compared in Table 1.

Table 1. Lattice Parameters of the Two Unit Cells in the Experimental and Modeled Assemblies

	unit cell 1		unit cell 2	
	experimental	modeled	experimental	modeled
$a/\text{\AA}$	52 ± 1	55.3	14 ± 1	13.8
$b/\text{\AA}$	14 ± 1	13.8	14 ± 1	13.8
$\alpha/^\circ$	88 ± 1	83.0	88 ± 1	88.5
$\beta/^\circ$	$61.5 \pm 1.7^\circ$	$62.0 \pm 0.57^\circ$	$61.5 \pm 1.7^\circ$	$62.0 \pm 0.57^\circ$

The lattice parameters of the experimental and simulated assemblies show an excellent agreement. The slight deviation found for unit cell 1 could be explained since mobile solvent molecules are included in the unit cell. Unit cell 2 is constituted of PbPc molecules only and the lattice parameters of the modeled assembly agree even better with the experimental values. These calculated parameters also show an excellent agreement with the experimental measurements for PbPc assemblies formed in high vacuum.⁴⁹ Through these comparisons, a convincing match between the experimental and modeled assembly is found, which confirms the accurate description of the PbPc assembly by our model. This model also includes the solvent coadsorption, leading to the special alternating row arrangement observed in the experiments. This specific "single row-double row" organization is considered to stem from a possible better registry between PbPc rows and the

HOPG substrate when adsorbed in this periodicity. Although direct observation of solvent molecules by STM is always challenging because of their high mobility, in our experiments, bright wavy stripes between PbPc molecular rows are imaged occasionally. One example is shown in Figure S10a. Based on the structural model we built for the assembly (Figure S10b), those stripes are interpreted to be coadsorbed solvent molecules. This further confirms the solvent coadsorbed model built to explain the experimental assembly. The fact that solvent molecules can coadsorb within the assembly network could in principle provide a possibility to control the width of the gap between PbPc rows. Nevertheless, the coadsorption of solvent molecules is rather difficult to control, which precludes its further use as a design strategy in real experiments. Within these assemblies, HA molecules coadsorb with their alkyl chains parallel to the PbPc rows. Therefore, the gap width between PbPc rows is not expected to change even if a solvent with longer alkyl chains is employed.

3.3. Simulations of SIP Growth. The specific alternating row arrangement observed in the PbPc monolayers formed from solution has been explained by solvent coadsorption. However, in order to investigate whether a thin film growing from a monolayer could generate the known bulk polymorphs or a SIP of PbPc, we remove the solvent molecules and build compact PbPc multilayer assemblies. This choice is based on the fact that multilayer formation is rarely observed at the solution/substrate interface and is more relevant to deposition under dry conditions (e.g., by vacuum sublimation). Top and side views of the optimized atomistic model for the compact monolayer assembly are shown in Figure 5a,b respectively.

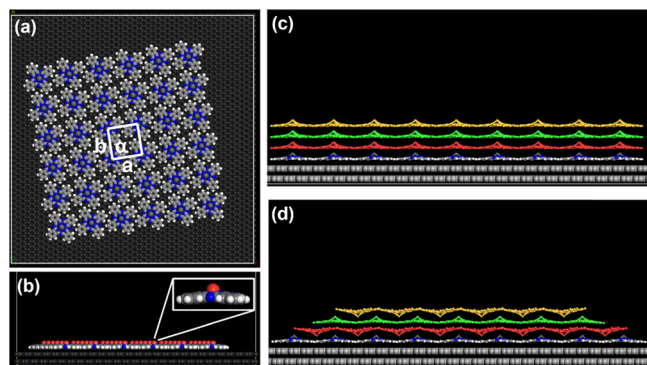


Figure 5. (a) Top view of the optimized compact PbPc assembly. Unit cell parameters: $a = b = 13.7$ Å and $\alpha = 90^\circ$. These parameters agree well with the PbPc assemblies deposited in high vacuum.⁴⁹ (b) Side view of the compact PbPc assembly after optimization, where all molecules are in the Pb-up conformation as shown in the zoomed image of one PbPc molecule. All Pb atoms are red-colored for better visualization. (c) Multilayer structure of PbPc grown from the compact assembly in columnar stacking. (d) Multilayer structure of PbPc grown from its compact assembly in alternating stacking. PbPc molecules in different layers are colored differently.

In this compact monolayer assembly, all PbPc molecules have the preferential Pb-up conformation. They stay on the same plane owing to the geometric 2D confinement exerted by the flat HOPG substrate. However, such an organization is not present in either the bulk monoclinic⁵⁰ or the triclinic⁵¹ phase of PbPc, which indicates the possibility to grow a SIP of PbPc from this assembly instead of generating the known bulk phases directly. The growth of an SIP is first studied in simulations, where it is

modeled by successive adsorption of up to four molecular layers. Here, two possible structures are proposed: columnar stacking (Figure 5c) and alternating stacking (Figure 5d).

Columnar stacking is similar to the bulk monoclinic phase of PbPc except that all PbPc molecules keep the same orientation. As for the alternating stacking, molecules in adjacent layers have different orientations and are packed alternately in either “face to face” (e.g., between the 1st and 2nd layers) or “back to back” (e.g., between the 2nd and 3rd layers) arrangement. The existence of such alternating stacking is deduced from spectroscopic measurements on a PbPc bilayer structure,^{66,67} but no experimental information exists on thicker multilayer structures.

Preliminary MM simulations indicate that the alternating stacking structure is more stable than its columnar counterpart (see Supporting Information for more details). Based on these findings, the alternating stacking of PbPc was further refined by the quench MD. The most stable final structure is depicted in Figure 6a,b, together with the extracted unit cell of the possible SIP.

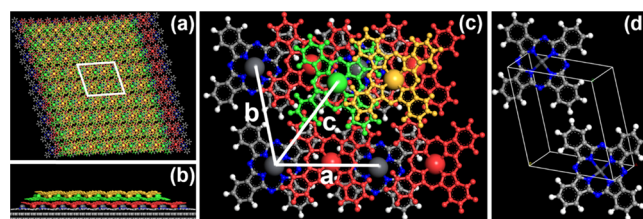


Figure 6. (a) Top view of the refined alternating-stacked PbPc multilayer. (b) Side view of the alternating-stacked PbPc multilayer after refinement. (c) Zoomed image of the region marked by the white parallelogram in panel (a), which shows a more detailed molecular arrangement and three lattice parameters to define the SIP. (d) Unit cell of the PbPc proposed SIP after Niggli cell reduction.

The interaction energies between neighboring molecular layers are summarized in Table 2 (see the Supporting Information for more details on the estimation of these energies).

Table 2. Interaction Energy (per Molecule) between Neighboring Layers in the Refined Alternating Stacking of PbPc

	interaction energy per molecule (kcal/mol)
1st layer and HOPG	−72.9
2nd and 1st layers	−58.1
3rd and 2nd layers	−53.5
4th and 3rd layers	−58.6

The calculation shows the existence of a stronger interaction between “face to face” stacked molecules. This provides a solid indication for the bilayer growth mechanism assumed in the experimental studies^{67,68} based on which the PbPc thin film grows per “face to face” and stacked dimer and molecules have alternating orientations in adjacent layers. It is revealed by these force field simulations that the alternating stacking shows superior structural rigidity and stability. It is therefore reasonable to hypothesize that a possible PbPc SIP would grow in this alternating packing manner.

Figure 6c shows the enlarged central region of the modeled multilayer, which is marked by the white parallelogram in Figure

6a. The color code for molecules belonging to different layers is the same as above: molecules in the second, third, and fourth layers are colored in red, green, and orange, respectively. It is very clear that in this refined structure, molecules in different layers have the same orientation, which makes it feasible to define a unit cell for the SIP from this multilayer structure. The three lattice parameters a , b , and c of the SIP are illustrated in Figure 6c. The Niggli cell reduction is then performed to improve the highly skewed cell that is extracted directly from the multilayer structure. After reduction, a triclinic unit cell belonging to the $P-1$ space group is obtained for the SIP (Figure 6d). There are two molecules within the unit cell and the lattice parameters are $a = 7.70 \text{ \AA}$, $b = 12.23 \text{ \AA}$, $c = 13.3 \text{ \AA}$, $\alpha = 71.39^\circ$, $\beta = 80.70^\circ$, and $\gamma = 78.09^\circ$. The density of this predicted SIP unit cell is 1.91 g/cm^3 , which is only 1 and 2.5% lower than the values for the bulk triclinic and monoclinic phases of PbPc, respectively. Such a difference is quite reasonable when comparing the density of SIPs and bulk polymorphs for a given compound.

3.4. Experimental Crystal Structure Determination for PbPc Thin Films. In parallel to the simulations, specular X-ray diffraction and GIXD measurements were performed on PbPc thin films deposited on graphite by vacuum sublimation; the typical thickness of these samples is in the 20–40 nm range. Although the PbPc thin films are prepared under the dry conditions instead of the solution environment as the SAMN, it is reasonable to hypothesize, based on the reported STM studies,⁴⁹ that the first molecular layer adsorbs on the substrate in the Pb-up conformation, similar to the self-assembly from solution. Specular X-ray diffraction measurements were first performed to probe the out-of-plane periodicities of the thin films. The result is depicted in Figure 7a.

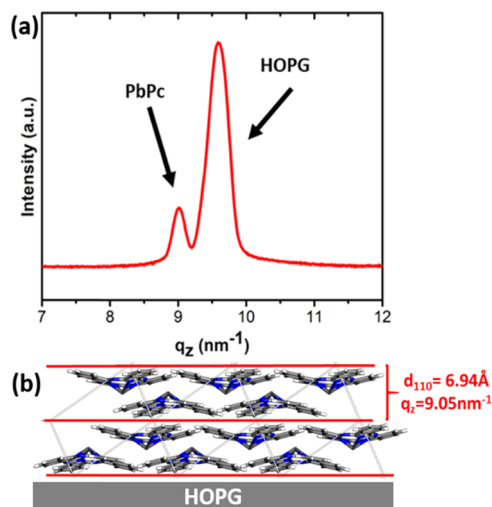


Figure 7. (a) Specular X-ray diffraction pattern of a PbPc thin film with a thickness of $\sim 40 \text{ nm}$. (b) Molecular model showing the simulated SIP in the orientation determined by the specular X-ray diffraction: the (110) plane of the simulated SIP is parallel to the substrate, with $d_{110} = 6.94 \text{ \AA}$ and corresponding $q_z = 9.05 \text{ nm}^{-1}$.

Diffraction peaks were found at $q_z = 9.01$ and 9.48 nm^{-1} , which correspond to d -spacings of 6.97 and 6.63 \AA , respectively. The d -spacing of the first peak is in excellent agreement with the interplanar distance of the (110) planes ($d_{110} = 6.94 \text{ \AA}$) of the simulated SIP. The second peak at 9.48 nm^{-1} (6.63 \AA) is related to the HOPG substrate. The preferred orientation of the crystallites within the thin film could be accordingly determined:

the (110) plane of the simulated SIP is parallel to the substrate. With this orientation, the C_4 symmetry axis of the PbPc molecules is perpendicular to the substrate, as shown in Figure 7b.

After the out-of-plane order of the thin films is determined by the specular X-ray diffraction, the in-plane order is probed by GIXD (Figure 8). Strong and clear Bragg peaks in the pattern

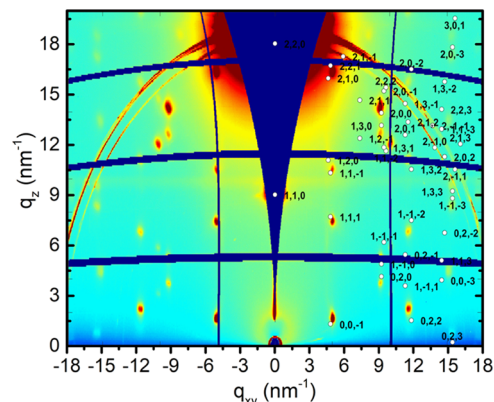


Table 3. Unit Cell Parameters of the SIP Determined from Molecular Modeling and an Experimental Pattern

	molecular model prediction	experimental determination
$a/\text{\AA}$	7.70	8.14
$b/\text{\AA}$	13.23	12.86
$c/\text{\AA}$	13.30	13.03
$\alpha/^\circ$	71.39	68.41
$\beta/^\circ$	80.70	80.95
$\gamma/^\circ$	78.09	81.21
$V/\text{\AA}^3$	1250	1245.8

between these two unit cells is only 0.8 kcal/mol; in other words, these two unit cells are energetically equivalent. The crystal structure information file (cif) of the optimized molecular packing can be found in the [Supporting Information](#) as well as in the Cambridge Structural Database under reference number 2121171.

Figure 9 shows the experimental GIXD map together with a calculated peak pattern on the basis of the adapted SIP with its

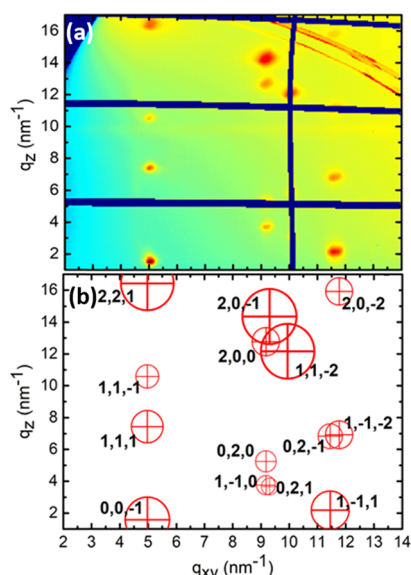


Figure 9. (a) GIXD map of a 40 nm-thick PbPc film on HOPG measured at an incidence angle of 0.5° and (b) the calculated peak positions (red crosses) of the adapted SIP in the 110 orientation and the determined squared structure factors (red circles); the size of the circles corresponds to the calculated intensities normalized to the highest value.

(110) plane parallel to the substrate. In panel (b), the theoretical peak positions are marked with red crosses while the squared structural factor of each peak is proportional to the area of the associated circle. We observe excellent matching with the experimental peak intensities. As the structural factors are directly related to the molecular arrangement within the crystal lattice, this demonstrates that the packing of PbPc molecules within the thin films is the same as in the proposed SIP unit cell. Based on the excellent agreement of both the peak positions and intensities, it can be concluded that the crystal structure of the PbPc thin films is successfully predicted by the molecular modeling, pointing to the existence of a previously unknown SIP for PbPc.

4. CONCLUSIONS

In summary, the formation, structure, and stability of an SIP in a prototypical molecular semiconductor, PbPc, were understood in detail. In classical crystal structure prediction (CSP) calculations, the effects of substrate are not considered, which makes it difficult to predict SIPs using CSP. Here we started from the substrate surface by investigating first the formation of SAMNs of PbPc at the solvent/graphite interface. The adsorption conformation of the PbPc molecules within the monolayer was ascertained by combining STM experiments, STM image simulations, and atomistic MM/MD simulations. The nonplanarity of the PbPc molecule appears as a major feature affecting the structural characteristics of the monolayer, which has the potential to direct the following crystal growth.

Our study was then extended to explore the structure of PbPc multilayers on the HOPG substrate in order to mimic the growth of thin crystalline films. The growth of a new SIP for PbPc was successfully modeled by the force field simulations, and the prediction of that SIP was proved to be successful compared to the crystal structure of PVD-prepared thin films. To our knowledge, this is the first SIP identified for PbPc.

Previous experimental studies have claimed that the origin of SIPs could be traced to the structure of the corresponding monolayer.⁶⁹ With the aim of going beyond a simple structural comparison between the monolayer and the SIP, we used a joint modeling/experimental approach to describe in detail the structure of the initial assembly and the formation and stability of the multilayer system leading to the SIP. With this approach, we reveal explicitly the detailed connection between the self-assembled monolayer and SIP templated by it. One major, initial aspect is that when the molecules assemble on the substrate, they adopt an organization that does not exist in the bulk polymorph. The second important aspect is to identify the interactions by which that new molecular organization is then able to template the subsequent crystal growth, leading to the formation of an SIP. Such a sequence may represent a typical growth mechanism for the SIPs. More generally, we believe that the bottom-up approach we propose here, where the substrate is explicitly involved and the formation of the SIP is followed layer by layer, shows strong potential for predicting SIPs of organic molecules, beyond the specific case described here.

To conclude, this study proposes a new methodology to generate SIPs for organic semiconducting materials using self-assembled monolayers as the template. With the help of a multiscale computational chemistry approach, the crystal structure of the SIP is successfully predicted a priori. Such an approach could then be used as a design strategy for crystal engineering of organic semiconducting materials in general. This is of prime importance for the technological applications of those materials since most molecular semiconducting devices rely on thin crystalline films as active layers and the key properties of those materials, in particular, the charge mobility, are very sensitive to the molecular packing in the thin films.

■ ASSOCIATED CONTENT

Supporting Information

The Supporting Information is available free of charge at <https://pubs.acs.org/doi/10.1021/acs.chemmater.1c04038>.

Additional information on large-scale STM images of a PbPc self-assembled monolayer; time-dependent STM images of PbPc formed at the HA/HOPG interface; Dreiding force field modification for PbPc; quench MD

simulations; PbPc assembly with coadsorbed solvent molecules; columnar stacking of PbPc molecules after optimization by MM; calculation of the interlayer interaction energy for the alternating stacking of PbPc; calculation of structural factors; and X-ray diffraction of PbPc deposited on graphene (PDF)

Crystal structure information file of the discovered PbPc SIP (CIF)

AUTHOR INFORMATION

Corresponding Author

Roberto Lazzaroni – Laboratory for Chemistry of Novel Materials, Materials Research Institute, University of Mons, 7000 Mons, Belgium; orcid.org/0000-0002-6334-4068; Email: Roberto.LAZZARONI@umons.ac.be

Authors

Yansong Hao – Laboratory for Chemistry of Novel Materials, Materials Research Institute, University of Mons, 7000 Mons, Belgium; Electron Microscopy for Materials Science (EMAT) and NANOlaboratory Center of Excellence, University of Antwerp, 2610 Antwerp, Belgium; orcid.org/0000-0001-8997-0430

Gangamallaiiah Velpula – Division of Molecular Imaging & Photonics, Department of Chemistry, KU Leuven-University of Leuven, 3001 Leuven, Belgium; orcid.org/0000-0002-0642-6892

Martin Kaltenecker – Institute of Solid State Physics, Graz University of Technology, Graz 8010, Austria; Laboratory of Polymer Chemistry, Faculty of Science, Université Libre de Bruxelles (ULB), 1050 Brussels, Belgium

Wolfgang Rao Bodlos – Institute of Solid State Physics, Graz University of Technology, Graz 8010, Austria; orcid.org/0000-0002-6187-5260

François Vibert – Laboratory of Polymer Chemistry, Faculty of Science, Université Libre de Bruxelles (ULB), 1050 Brussels, Belgium

Kunal S. Mali – Division of Molecular Imaging & Photonics, Department of Chemistry, KU Leuven-University of Leuven, 3001 Leuven, Belgium; orcid.org/0000-0002-9938-6446

Steven De Feyter – Division of Molecular Imaging & Photonics, Department of Chemistry, KU Leuven-University of Leuven, 3001 Leuven, Belgium; orcid.org/0000-0002-0909-9292

Roland Resel – Institute of Solid State Physics, Graz University of Technology, Graz 8010, Austria; orcid.org/0000-0003-0079-3525

Yves Henri Geerts – Laboratory of Polymer Chemistry, Faculty of Science, Université Libre de Bruxelles (ULB), 1050 Brussels, Belgium; International Solvay Institutes of Physics and Chemistry, ULB, 1050 Brussels, Belgium; orcid.org/0000-0002-2660-5767

Sandra Van Aert – Electron Microscopy for Materials Science (EMAT) and NANOlaboratory Center of Excellence, University of Antwerp, 2610 Antwerp, Belgium

David Beljonne – Laboratory for Chemistry of Novel Materials, Materials Research Institute, University of Mons, 7000 Mons, Belgium; orcid.org/0000-0002-2989-3557

Complete contact information is available at:

<https://pubs.acs.org/10.1021/acs.chemmater.1c04038>

Notes

The authors declare no competing financial interest.

ACKNOWLEDGMENTS

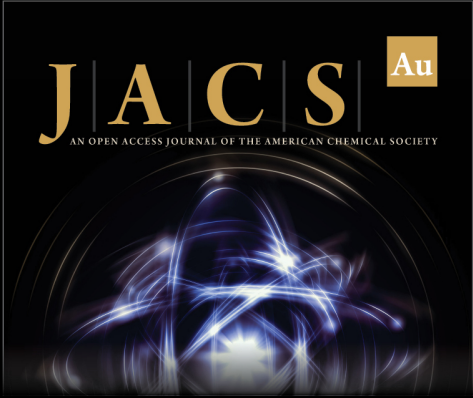
This work is supported by FWO and FNRS within the 2Dto3D project of the EOS program (grant number 30489208). The molecular modeling activities in Mons are supported by FNRS (Consortium des Equipements de Calcul Intensif – CÉCI, under Grant 2.5020.11) and by the Walloon Region (ZENOBÉ Tier-1 supercomputer, under grant 1117545). Y.G. is thankful to the Belgian National Fund for Scientific Research (FNRS) for financial support through research projects BTBT no. 2.4565.11, Phasetrans no. T.0058.14, and Pi-Fast no. T.0072.18. Financial supports from the French Community of Belgium (ARC n° 20061) and by the Walloon Region (WCS no. 1117306 and SOLIDYE no. 1510602) are also acknowledged. D.B. is an FNRS Research Director. G.M.V., K.S.M., and S.D.F. acknowledge support from FWO and KU Leuven-Internal Funds. The authors acknowledge Dr. D. Cornil for his assistance with the STM image simulations and the Synchrotron Elettra Trieste for allocation of synchrotron radiation and thank Luisa Barba for assistance in using beamline XRD1.

REFERENCES

- (1) Jones, A. O.; Chattopadhyay, B.; Geerts, Y. H.; Resel, R. Substrate-Induced and Thin-Film Phases: Polymorphism of Organic Materials on Surfaces. *Adv. Funct. Mater.* **2016**, *26*, 2233–2255.
- (2) Yoneya, M.; Kawasaki, M.; Ando, M. Are pentacene monolayer and thin-film polymorphs really substrate-induced? A molecular dynamics simulation study. *J. Phys. Chem. C* **2012**, *116*, 791–795.
- (3) Hilfiker, R. *Polymorphism in the pharmaceutical industry*; Wiley Online Library: 2006; Vol. 2.
- (4) Yoshida, H.; Inaba, K.; Sato, N. X-ray diffraction reciprocal space mapping study of the thin film phase of pentacene. *Appl. Phys. Lett.* **2007**, *90*, 181930.
- (5) Gbabode, G.; Dumont, N.; Quist, F.; Schweicher, G.; Moser, A.; Viville, P.; Lazzaroni, R.; Geerts, Y. H. Substrate-Induced Crystal Plastic Phase of a Discotic Liquid Crystal. *Adv. Mater.* **2012**, *24*, 658–662.
- (6) Blagden, N.; de Matas, M.; Gavan, P. T.; York, P. Crystal engineering of active pharmaceutical ingredients to improve solubility and dissolution rates. *Adv. Drug Delivery Rev.* **2007**, *59*, 617–630.
- (7) Ehmman, H. M.; Werzer, O. Surface mediated structures: stabilization of metastable polymorphs on the example of paracetamol. *Cryst. Growth Des.* **2014**, *14*, 3680–3684.
- (8) Zhang, K.; Fella, N.; Shtukenberg, A. G.; Fu, X.; Hu, C.; Ward, M. D. Discovery of new polymorphs of the tuberculosis drug isoniazid. *CrystEngComm* **2020**, *22*, 2705–2708.
- (9) Cruz-Cabeza, A. J.; Bernstein, J. Conformational polymorphism. *Chem. Rev.* **2014**, *114*, 2170–2191.
- (10) Nyman, J.; Day, G. M. Static and lattice vibrational energy differences between polymorphs. *CrystEngComm* **2015**, *17*, 5154–5165.
- (11) Bernstein, J. Polymorphism— a perspective. *Cryst. Growth Des.* **2011**, *11*, 632–650.
- (12) Salzmann, I.; Nabok, D.; Oehzelt, M.; Duhm, S.; Moser, A.; Heime, G.; Puschnig, P.; Ambrosch-Draxl, C.; Rabe, J. P.; Koch, N. Structure solution of the 6, 13-pentacenequinone surface-induced polymorph by combining X-ray diffraction reciprocal-space mapping and theoretical structure modeling. *Cryst. Growth Des.* **2011**, *11*, 600–606.
- (13) Schiefer, S.; Huth, M.; Dobrinevski, A.; Nickel, B. Determination of the crystal structure of substrate-induced pentacene polymorphs in fiber structured thin films. *J. Am. Chem. Soc.* **2007**, *129*, 10316–10317.
- (14) Pithan, L.; Nabok, D.; Cocchi, C.; Beyer, P.; Duva, G.; Simbrunner, J.; Rawle, J.; Nicklin, C.; Schäfer, P.; Draxl, C. Molecular structure of the substrate-induced thin-film phase of tetracene. *J. Chem. Phys.* **2018**, *149*, 144701.

- (15) Weissbuch, I.; Lahav, M.; Leiserowitz, L. Toward stereochemical control, monitoring, and understanding of crystal nucleation. *Cryst. Growth Des.* **2003**, *3*, 125–150.
- (16) Resel, R.; Koch, N.; Meghdadi, F.; Leising, G.; Athouel, L.; Froyer, G.; Hofer, F. A polymorph crystal structure of hexaphenyl observed in thin films. *Cryst. Res. Technol.* **2001**, *36*, 47–54.
- (17) Mänz, A.; Breuer, T.; Witte, G. Epitaxial Tetrathiafulvalene–Tetracyanoquinodimethane Thin Films on KCl (100): New Preparation Methods and Observation of Interface-Mediated Thin Film Polymorphism. *Cryst. Growth Des.* **2015**, *15*, 395–403.
- (18) Yang, J.; Erriah, B.; Hu, C. T.; Reiter, E.; Zhu, X.; López-Mejías, V.; Carmona-Sepúlveda, I. P.; Ward, M. D.; Kahr, B. A deltamethrin crystal polymorph for more effective malaria control. *Proc. Natl. Acad. Sci. U. S. A.* **2020**, *117*, 26633–26638.
- (19) Jones, A. O.; Geerts, Y. H.; Karpinska, J.; Kennedy, A. R.; Resel, R.; Röthel, C.; Ruzié, C.; Werzer, O.; Sferrazza, M. Substrate-induced phase of a [1] benzothieno [3, 2-b] benzothiophene derivative and phase evolution by aging and solvent vapor annealing. *ACS Appl. Mater. Interfaces* **2015**, *7*, 1868–1873.
- (20) Lercher, C.; Röthel, C.; Roscioni, O. M.; Geerts, Y. H.; Shen, Q.; Teichert, C.; Fischer, R.; Leising, G.; Sferrazza, M.; Gbabode, G. Polymorphism of dioctyl-terthiophene within thin films: The role of the first monolayer. *Chem. Phys. Lett.* **2015**, *630*, 12–17.
- (21) Mannsfeld, S. C.; Tang, M. L.; Bao, Z. Thin film structure of triisopropylsilyl ethynyl-functionalized pentacene and tetraceno [2, 3-b] thiophene from grazing incidence X-Ray diffraction. *Adv. Mater.* **2011**, *23*, 127–131.
- (22) Krauss, T. N.; Barrena, E.; Zhang, X. N.; De Oteyza, D. G.; Major, J.; Dehm, V.; Würthner, F.; Cavalcanti, L. P.; Dosch, H. Three-dimensional molecular packing of thin organic films of PTCDI-C8 determined by surface X-ray diffraction. *Langmuir* **2008**, *24*, 12742–12744.
- (23) Nabok, D.; Puschnig, P.; Ambrosch-Draxl, C.; Werzer, O.; Resel, R.; Smilgies, D.-M. Crystal and electronic structures of pentacene thin films from grazing-incidence x-ray diffraction and first-principles calculations. *Phys. Rev. B* **2007**, *76*, No. 235322.
- (24) Wu, J.; Spence, J. Electron diffraction of thin-film pentacene. *J. Appl. Crystallogr.* **2004**, *37*, 78–81.
- (25) Chou, W.-Y.; Chang, M.-H.; Cheng, H.-L.; Lee, Y.-C.; Chang, C.-C.; Sheu, H.-S. New pentacene crystalline phase induced by nanoimprinted polyimide gratings. *J. Phys. Chem. C* **2012**, *116*, 8619–8626.
- (26) Dimitrakopoulos, C.; Brown, A.; Pomp, A. Molecular beam deposited thin films of pentacene for organic field effect transistor applications. *J. Appl. Phys.* **1996**, *80*, 2501–2508.
- (27) Bouchoms, I.; Schoonveld, W.; Vrijmoeth, J.; Klapwijk, T. Morphology identification of the thin film phases of vacuum evaporated pentacene on SiO₂ substrates. *Synth. Met.* **1999**, *104*, 175–178.
- (28) Simões, R. G.; Salzmann, I.; Resel, R.; Röthel, C.; Geerts, Y. H. Stabilization of the Metastable Form I of Piracetam by Crystallization on Silicon Oxide Surfaces. *Cryst. Growth Des.* **2018**, *18*, 4123–4129.
- (29) Christian, P.; Röthel, C.; Tazreiter, M.; Zimmer, A.; Salzmann, I.; Resel, R.; Werzer, O. Crystallization of carbamazepine in proximity to its precursor iminostilbene and a silica surface. *Cryst. Growth Des.* **2016**, *16*, 2771–2778.
- (30) Jones, A. O.; Röthel, C.; Lassnig, R.; Bedoya-Martínez, O.; Christian, P.; Salzmann, I.; Kunert, B.; Winkler, A.; Resel, R. Solution of an elusive pigment crystal structure from a thin film: a combined X-ray diffraction and computational study. *CrystEngComm* **2017**, *19*, 1902–1911.
- (31) Yang, J.; Hu, C. T.; Zhu, X.; Zhu, Q.; Ward, M. D.; Kahr, B. DDT polymorphism and the lethality of crystal forms. *Angew. Chem. Int. Ed.* **2017**, *129*, 10299–10303.
- (32) Mali, K. S.; Pearce, N.; De Feyter, S.; Champness, N. R. Frontiers of supramolecular chemistry at solid surfaces. *Chem. Soc. Rev.* **2017**, *46*, 2520–2542.
- (33) Goronzy, D. P.; Ebrahimi, M.; Rosei, F.; Arramel, Fang, Y.; De Feyter, S.; Tait, S. L.; Wang, C.; Beton, P. H.; Wee, A. T. Supramolecular assemblies on surfaces: nanopatterning, functionality, and reactivity. *ACS Nano* **2018**, *12*, 7445–7481.
- (34) Tahara, K.; Furukawa, S.; Uji-i, H.; Uchino, T.; Ichikawa, T.; Zhang, J.; Mamdouh, W.; Sonoda, M.; De Schryver, F. C.; De Feyter, S. Two-dimensional porous molecular networks of dehydrobenzo [12] annulene derivatives via alkyl chain interdigitation. *J. Am. Chem. Soc.* **2006**, *128*, 16613–16625.
- (35) Elemans, J. A.; Lei, S.; De Feyter, S. Molecular and Supramolecular Networks on Surfaces: From Two-Dimensional Crystal Engineering to Reactivity. *Angew. Chem., Int. Ed.* **2009**, *48*, 7298–7332.
- (36) Gutzler, R.; Fu, C.; Dadvand, A.; Hua, Y.; MacLeod, J. M.; Rosei, F.; Perepichka, D. F. Halogen bonds in 2D supramolecular self-assembly of organic semiconductors. *Nanoscale* **2012**, *4*, S965–S971.
- (37) Kim, M. K.; Xue, Y.; Pašková, T.; Zimmt, M. B. Monolayer patterning using ketone dipoles. *Phys. Chem. Chem. Phys.* **2013**, *15*, 12466–12474.
- (38) Steeno, R.; Minoia, A.; Gimenez-Lopez, M. C.; Blunt, M. O.; Champness, N. R.; Lazzaroni, R.; Mali, K. S.; De Feyter, S. Molecular dopant determines the structure of a physisorbed self-assembled molecular network. *Chem. Commun.* **2021**, *57*, 1454–1457.
- (39) Mali, K. S.; Adisojoso, J.; Ghijsens, E.; De Cat, I.; De Feyter, S. Exploring the complexity of supramolecular interactions for patterning at the liquid–solid interface. *Acc. Chem. Res.* **2012**, *45*, 1309–1320.
- (40) MacLeod, J. M.; Ivasenko, O.; Fu, C.; Taerum, T.; Rosei, F.; Perepichka, D. F. Supramolecular ordering in oligothiophene–fullerene monolayers. *J. Am. Chem. Soc.* **2009**, *131*, 16844–16850.
- (41) Korolkov, V. V.; Svatek, S. A.; Summerfield, A.; Kerfoot, J.; Yang, L.; Taniguchi, T.; Watanabe, K.; Champness, N. R.; Besley, N. A.; Beton, P. H. van der Waals-induced chromatic shifts in hydrogen-bonded two-dimensional porphyrin arrays on boron nitride. *ACS Nano* **2015**, *9*, 10347–10355.
- (42) Blunt, M. O.; Russell, J. C.; del Carmen Gimenez-Lopez, M.; Taleb, N.; Lin, X.; Schröder, M.; Champness, N. R.; Beton, P. H. Guest-induced growth of a surface-based supramolecular bilayer. *Nat. Chem.* **2011**, *3*, 74–78.
- (43) Hamamoto, N.; Sonoda, H.; Sumimoto, M.; Hori, K.; Fujimoto, H. Theoretical study on crystal polymorphism and electronic structure of lead (ii) phthalocyanine using model dimers. *RSC Adv.* **2017**, *7*, 8646–8653.
- (44) Kumar, T. M.; Achar, B. Synthesis and characterization of lead phthalocyanine and its derivatives. *J. Organomet. Chem.* **2006**, *691*, 331–336.
- (45) Yoshida, Y.; Tanigaki, N.; Yase, K. Evaluation of Thin Films of Functional Organic Materials by Total Reflection X-Ray Diffraction. *Mol. Cryst. Liq. Cryst. Sci. Technol., Sect. A* **1996**, *280*, 271–276.
- (46) Collins, R.; Belghachi, A. Structural properties of lead phthalocyanine thin films. *Mater. Lett.* **1989**, *8*, 349–352.
- (47) Heilmann, A.; Müller, M.; Hamann, C.; Lantto, V.; Torvela, H. Gas sensitivity measurements on NO₂ sensors based on lead phthalocyanine thin films. *Sens. Actuators, B* **1991**, *4*, 511–513.
- (48) Strohmaier, R.; Ludwig, C.; Petersen, J.; Gompf, B.; Eisenmenger, W. Scanning tunneling microscope investigations of lead–phthalocyanine on MoS₂. *J. Vac. Sci. Technol. B* **1996**, *14*, 1079–1082.
- (49) Nguyen, T. N.; Aprojanz, J.; Jäger, M.; Nguyen, T. H.; Tegenkamp, C. Noninvasive coupling of PbPc monolayers to epitaxial graphene on SiC (0001). *Surf. Sci.* **2019**, *686*, 45–51.
- (50) Ukei, K. Lead phthalocyanine. *Acta Crystallogr. B* **1973**, *29*, 2290–2292.
- (51) Iyechika, Y.; Yakushi, K.; Ikemoto, I.; Kuroda, H. Structure of lead phthalocyanine (triclinic form). *Acta Crystallogr. B* **1982**, *38*, 766–770.
- (52) Schrode, B.; Pachmajer, S.; Dohr, M.; Röthel, C.; Domke, J.; Fritz, T.; Resel, R.; Werzer, O. GIDVis: a comprehensive software tool for geometry-independent grazing-incidence X-ray diffraction data analysis and pole-figure calculations. *J. Appl. Crystallogr.* **2019**, *52*, 683–689.

- (53) Kainz, M. P.; Legenstein, L.; Holzer, V.; Hofer, S.; Kaltenegger, M.; Resel, R.; Simbrunner, J. GIDInd: an automated indexing software for grazing-incidence X-ray diffraction data. *J. Appl. Crystallogr.* **2021**, *54*, 1256–1267.
- (54) Simbrunner, J.; Simbrunner, C.; Schrode, B.; Röthel, C.; Bedoya-Martinez, N.; Salzmann, I.; Resel, R. Indexing of grazing-incidence X-ray diffraction patterns: the case of fibre-textured thin films. *Acta Crystallogr. A* **2018**, *74*, 373–387.
- (55) Soler, J. M.; Artacho, E.; Gale, J. D.; García, A.; Junquera, J.; Ordejón, P.; Sánchez-Portal, D. The SIESTA method for ab initio order-N materials simulation. *J. Phys.: Condens. Matter* **2002**, *14*, 2745.
- (56) Troullier, N.; Martins, J. L. Efficient pseudopotentials for plane-wave calculations. *Phys. Rev. B* **1991**, *43*, 1993.
- (57) Grimme, S. Semiempirical GGA-type density functional constructed with a long-range dispersion correction. *J. Comput. Chem.* **2006**, *27*, 1787–1799.
- (58) Horcas, I.; Fernández, R.; Gomez-Rodriguez, J.; Colchero, J.; Gómez-Herrero, J.; Baro, A. WSXM: a software for scanning probe microscopy and a tool for nanotechnology. *Rev. Sci. Instrum.* **2007**, *78*, No. 013705.
- (59) BIOVIA, Dassault Systèmes. *BIOVIA Materials Studio*, 2018; Dassault Systèmes: San Diego, 2018.
- (60) Mayo, S. L.; Olafson, B. D.; Goddard, W. A. DREIDING: a generic force field for molecular simulations. *J. Phys. Chem.* **1990**, *94*, 8897–8909.
- (61) Frisch, M. J.; Trucks, G. W.; Schlegel, H. B.; Scuseria, G. E.; Robb, M. A.; Cheeseman, J. R.; Scalmani, G.; Barone, V.; Petersson, G. A.; Nakatsuji, H., et al. *Gaussian 16 Rev. C.01*. 2016.
- (62) Samoletov, A. A.; Dettmann, C. P.; Chaplain, M. A. Thermostats for “slow” configurational modes. *J. Stat. Phys.* **2007**, *128*, 1321–1336.
- (63) Mali, K. S.; Zöphel, L.; Ivasenko, O.; Müllen, K.; De Feyter, S. Manifestations of Non-Planar Adsorption Geometries of Lead Pyrenocyanine at the Liquid-Solid Interface. *Chem. – Asian J.* **2013**, *8*, 2497–2505.
- (64) Lackinger, M.; Hietschold, M. Determining adsorption geometry of individual tin–phthalocyanine molecules on Ag (111)—a STM study at submonolayer coverage. *Surf. Sci.* **2002**, *520*, L619–L624.
- (65) Sirtl, T.; Song, W.; Eder, G.; Neogi, S.; Schmittl, M.; Heckl, W. M.; Lackinger, M. Solvent-dependent stabilization of metastable monolayer polymorphs at the liquid–solid interface. *ACS Nano* **2013**, *7*, 6711–6718.
- (66) Kashimoto, Y.; Yonezawa, K.; Meissner, M.; Gruenewald, M.; Ueba, T.; Kera, S.; Forker, R.; Fritz, T.; Yoshida, H. The evolution of intermolecular energy bands of occupied and unoccupied molecular states in organic thin films. *J. Phys. Chem. C* **2018**, *122*, 12090–12097.
- (67) Kera, S.; Fukagawa, H.; Kataoka, T.; Hosoumi, S.; Yamane, H.; Ueno, N. Spectroscopic evidence of strong π – π interorbital interaction in a lead-phthalocyanine bilayer film attributed to the dimer nanostructure. *Phys. Rev. B* **2007**, *75*, No. 121305.
- (68) Yamane, H.; Honda, H.; Fukagawa, H.; Ohya, M.; Hinuma, Y.; Kera, S.; Okudaira, K.; Ueno, N. HOMO-band fine structure of OTi- and Pb-phthalocyanine ultrathin films: effects of the electric dipole layer. *J. Electron Spectrosc. Relat. Phenom.* **2004**, *137*, 223–227.
- (69) Fu, C.; Lin, H.-p.; Macleod, J. M.; Krayev, A.; Rosei, F.; Perepichka, D. F. Unravelling the self-assembly of hydrogen bonded NDI semiconductors in 2D and 3D. *Chem. Mater.* **2016**, *28*, 951–961.



JACS Au
AN OPEN ACCESS JOURNAL OF THE AMERICAN CHEMICAL SOCIETY

Editor-in-Chief
Prof. Christopher W. Jones
Georgia Institute of Technology, USA

Open for Submissions

pubs.acs.org/jacsau

ACS Publications
Most Trusted. Most Cited. Most Read.